Journal of Power Sources 190 (2009) 447–452

Contents lists available at ScienceDirect

Journal of Power Sources

journal homepage: www.elsevier.com/locate/jpowsour

ZnO-doped $BaZr_{0.85}Y_{0.15}O_{3-\delta}$ proton-conducting electrolytes: Characterization and fabrication of thin films

Cheng Peng[1], Juri Melnik, Jinxia Li, Jingli Luo*, Alan R. Sanger, Karl T. Chuang

Department of Chemical and Materials Engineering, University of Alberta, Edmonton, AB, Canada T6G 2G6

ARTICLE INFO

Article history:
Received 29 November 2008
Received in revised form 11 January 2009
Accepted 12 January 2009
Available online 20 January 2009

Keywords:
ZnO-doped $BaZr_{0.85}Y_{0.15}O_{3-\delta}$ perovskite electrolyte
Solid oxide fuel cells
Proton-conducting solid oxide electrolytes
Thin film electrolytes
Sintering

ABSTRACT

ZnO-doped $BaZr_{0.85}Y_{0.15}O_{3-\delta}$ perovskite oxide sintered at 1500 °C has bulk conductivity of the order of 10^{-2} S cm^{-1} above 650 °C, which makes it an attractive proton-conducting electrolyte for intermediate-temperature solid oxide fuel cells. The structure, morphology and electrical conductivity of the electrolyte vary with sintering temperature. Optimal electrochemical performance is achieved when the sintering temperature is about 1500 °C. Cathode-supported electrolyte assemblies were prepared using spin coating technique. Thin film electrolytes were shown to be dense using SEM and EDX analyses.

1. Introduction

Proton-conducting oxide electrolytes for intermediate-temperature solid oxide fuel cells (IT-SOFCs) have drawn much attention since the first reports by Iwahara et al. [1–3]. Yttrium doped barium zirconates are among the most promising IT proton conductors due to their relatively high conductivity and chemical stability. The conductivity of such materials is primarily protonic over a relatively wide range of temperature and oxygen partial pressures, without significant contributions from either oxide ionic or electronic conductivity [4–6]. However, there are significant differences in reported values for conductivities of $BaZr_{1-x}Y_xO_{3-\delta}$ [7–10], which appear to be related to use of different synthesis procedures. Indeed, the zirconates do not sinter easily, and the highest conductivities reported previously were obtained only when sintering was performed about 1700 °C, which is a major obstacle for application of $BaZrO_3$-based proton conductors.

It has been proposed by Snijkers et al. [11] that the achievement of the highest conductivities is effected by some form of phase transformation or segregation and/or by a slow kinetic process of water absorption. Furthermore, Kreuer et al. [12] have shown that the conductivity of doped barium cerates held at elevated temperatures for long periods of time can drop by as much as two orders of magnitude. They attributed this drop to loss of BaO through evaporation. Shima and Haile [13] also attributed the approximately 2 wt% weight loss upon sintering at 1650 °C to BaO evaporation. Regardless of the cause or mechanism, it is apparent that variations in stoichiometry have a significant influence on the conductivity of doped barium zirconate. Major barium loss can and does occur mainly at high temperatures. Therefore careful control of sintering parameters is necessary to obtain desired stoichiometry and reproducible properties.

Several methods have been proven effective for sintering ceramic materials at a lower temperature, and these can be classified into two categories: (i) use of powders having fine, narrow size distributions, prepared by various methods (hydrothermal synthesis [14,15], oxalate co-precipitation [16,17], chemical combustion synthesis [18], intensive mechanical milling [19], etc.); and (ii) addition of sintering promoters or aids. Starting with fine powder is helpful for densification at a lower heating temperature because of the increased driving force for sintering. However, formation of small sized pores between ultra-fine particles produces a high capillary force in the powder compact, which can result in low packing density and cracks formed during drying and firing [20]. Addition of sintering aids including widely used B_2O_3 [21–23], CuO [24–26], ZnO [27–30], etc. can promote ceramics densification and control grain growth during the sintering process.

Herein we describe use of ZnO sintering aid to achieve higher densification of $BaZr_{0.85}Y_{0.15}O_{3-\delta}$ (BZY15) at lower sintering temperatures. A wide range of sintering temperatures (1350–1500 °C)

* Corresponding author. Tel.: +1 780 492 2232.
E-mail address: jingli.luo@ualberta.ca (J. Luo).
[1] Permanent address: School of Chemistry and Chemical Engineering, South China University of Technology, Guangzhou 510641, China.

0378-7753/$ – see front matter © 2009 Elsevier B.V. All rights reserved.
doi:10.1016/j.jpowsour.2009.01.020

was chosen to examine the evolved microstructure and its effect on the electrochemical parameters. Pre-sintering of substrates and spin coating technique were performed to provide dense thin films with good compatibility to substrates on which they are deposited.

2. Experimental

2.1. Materials preparation and characterization

$BaZr_{0.85}Y_{0.15}O_{3-\delta}$ ceramic powder was synthesized by solid-state reaction using as the starting materials $BaCO_3$ (Aldrich) and nano-powders of ZrO_2 and Y_2O_3 (Inframat Advanced Materials). The powders were mixed in the required stoichiometry and ground in a planetary ball mill with isopropanol (IPA) for 24 h, then dried. ZrO_2 balls were used to reduce the chance of adventitious milling effects. The dried powders were ground in an agate mortar and calcined in air at 1450 °C for 10 h. Then 1 wt% of ZnO powder (Aldrich) was admixed to the calcined powders and the mixture was ball-milled for a further 24 h before the second calcination at 1450 °C for 10 h to form ZnO-doped BZY15 (BZY-Zn). The calcined samples were ball-milled and pressed uni-axially into disk pellets by hydrostatic pressing at 10 t in^{-2}. The pellets then were sintered in air at different temperatures in the range of 1350–1500 °C. Densities of the as-prepared pellets were measured using the Archimedes principle in deionized water. The densities of the well-sintered disks each were more than 95% of the theoretical density.

Crystal phase identification of synthesized materials was performed using a Siemens D5000 X-ray diffractometer with Ni filtered Co K_α radiation. Morphology and microstructure of the samples as well as elemental analysis were determined using SEM/EDX technique using a Hitachi S-2700 scanning electron microscope and PGT Imix system with a PRISM IG.

2.2. Slurry preparation and spin coating

Suspensions of BZY-Zn were prepared using an azeotropic mixture of reagent grade ethanol (Fisher scientific) and o-xylene (Sigma–Aldrich). The powder was mixed with the organic solvents and treated ultrasonically for 1 h. Prior to coating, the slurry was kept still for about 2 h in vacuum to remove air entrapped in the slurry during ultrasonification. The spin coating procedure was performed sequentially several times in order to obtain dense and uniform thin films having prescribed thicknesses. The samples were allowed to dry overnight at room temperature before they were sintered.

2.3. Fuel cell assembly

Platinum wires and meshes were used at both electrodes as output terminals and current collectors. The test station was used to operate fuel cells at temperatures as high as 900 °C with the fuel cell in either vertical or horizontal orientation. As described previously [31], the anode and cathode gas chambers were formed by placing the membrane electrode assembly (MEA) between coaxial pairs of alumina tubes, and the assembly was heated in a Thermolyne F79300 tubular furnace.

2.4. Conductivity and fuel cell performance measurements

In all tests a Solartron Electrochemical interface (S1 1287 and 1260) was used to monitor the open circuit voltage (OCV) between anode and cathode, and to measure current–potential performance and electrochemical impedance. Potentiodynamic mode was used when performing current–potential measurements at a scanning rate of 5 mV s^{-1}. The proton transport numbers were estimated from the EMF of hydrogen concentration cell measurements in the temperature region of 500–800 °C. The following electrochemical cell was assembled: gas (I), Pt|electrolyte|Pt, gas (II). For the hydrogen concentration cells, pure H_2 and 2% H_2 diluted with argon were used as gas (I) and gas (II), respectively. Impedance data typically were obtained over the frequency range 1 MHz to 0.1 Hz. The cell was allowed to equilibrate and stabilize for at least 1 h after each change in operating conditions before conducting further measurements.

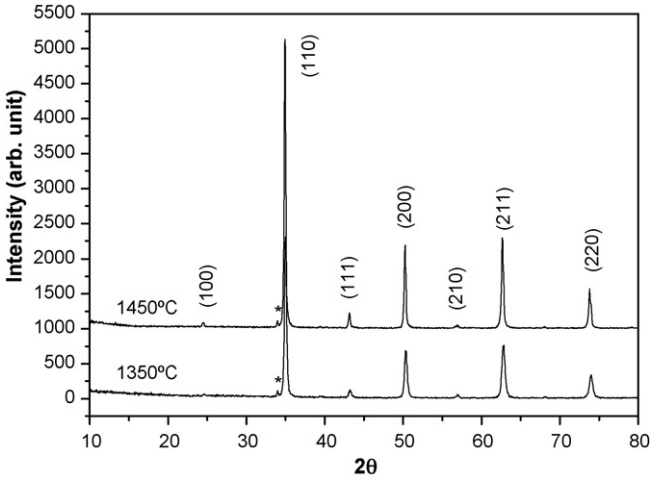

Fig. 1. XRD patterns of BZY-Zn powders calcined for 10 h at different temperatures (asterisk represents the impurity phase).

3. Results and discussion

3.1. Structure, morphology and conductivity of ZnO-doped BZY15

Typical XRD patterns of the BZY-Zn ceramic powders synthesized using solid-state reactions at different temperatures are shown in Fig. 1. The powders mainly consisted of single-phase cubic perovskite structure and there were no diffraction peaks corresponding to any of $BaCO_3$, ZrO_2 or ZnO. Fig. 1 also shows a peak arising from a small amount of impurity that cannot be indexed by pure $BaZrO_3$ phase (JCPDS card no. 06-0399), but which may be the strongest (2 2 2) diffraction peak of Y_2O_3 (JCPDS card no. 41-1105), thus indicating the presence of traces of Y_2O_3 in the mixture. The presence of Y_2O_3 impurity in the $BaZr_{1-x}Y_xO_{3-\delta}$ perovskite oxides was also observed by other authors firing at a higher temperature [6], which was attributed to the evaporation of some BaO on firing.

Cross-sectional SEM micrographs of the sintered membranes are shown in Fig. 2. It can be seen that BZY-Zn membranes are well-sintered even at temperatures as low as 1350 °C (Fig. 2d). However, in this case the grain size is almost the same as that of ball-milled powders, between 1 μm and 2 μm. The grain size increased with sintering temperature from ca. 1 μm (1350 °C, Fig. 2d) to ca. 4 μm (1500 °C, Fig. 2a), which made the membranes denser. The grain size increase with the T is due to a coalescence effect.

Normally, impedance spectrum can resolve the bulk, grain boundary and electrode/electrolyte interface processes from high frequency to low-frequency for ceramic electrolytes. Fig. 3 shows typical impedance spectrum over the range of 10^6 to 10^{-1} Hz for BZY-Zn at 550 °C. The high and mid frequency arcs overlapped to produce an exaggerated flattened semicircle. The first semicircle characteristically showed nanoFarad (nF) capacitance value and corresponded to grain boundaries resistance. The first intersection at the high frequency end was taken as the value of bulk resistance. The low-frequency behavior in the spectrum represented the behavior occurring at the electrolyte–electrode interface. The impedance spectra at different temperatures were modeled using

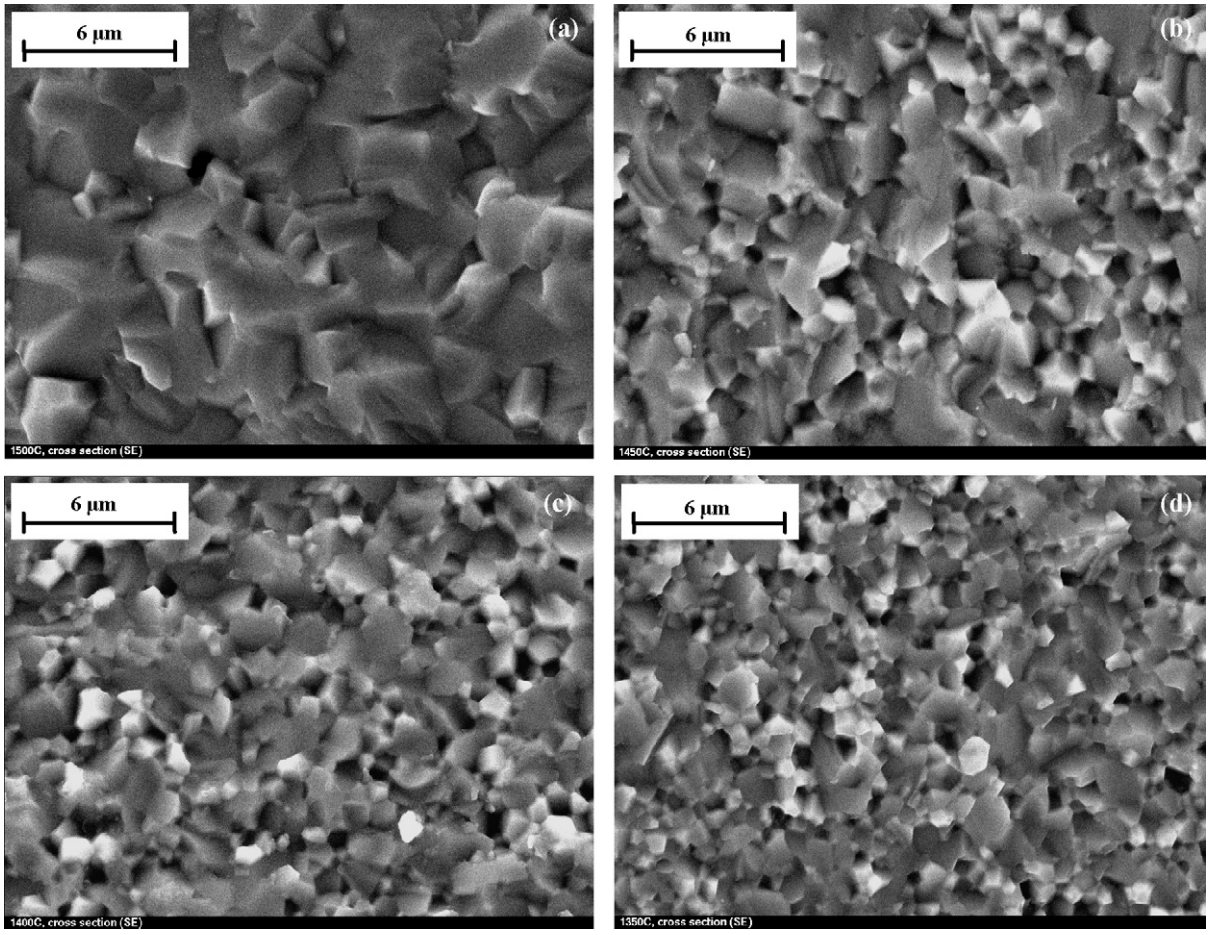

Fig. 2. Cross-sectional SEM images of BZY-Zn sintered at (a) 1500 °C; (b) 1450 °C; (c) 1400 °C; and (d) 1350 °C.

Zview software and the equivalent circuit shown in Fig. 3. This equivalent circuit model provided results that were consistent with the experimental impedance data. According to this model, the resistance values (grain bulk resistance, R_b and grain boundary resistance, R_{gb}) can be obtained from the intercepts of the arcs with the real impedance axis. Conductivity (σ) data for both R_b and R_{gb} are summarized in the form of Arrhenius plots in Fig. 4.

The BZY-Zn samples sintered at 1450 °C and 1500 °C exhibited bulk activation energy values (0.31 eV) similar to that for ZnO-free BZY15 sintered at 1650 °C (0.37 eV) [32]. However, samples of BZY-Zn sintered at 1500 °C exhibited much lower grains boundary activation energy values (about 0.31 eV) than pure BZY15 sintered at 1650 °C (1.07 eV) [32]. This suggests that the lower grains boundary resistance and activation energy for BZY-Zn sintered at 1500 °C is attributable to increased grain size, and the consequent improved grain development and decreased grain boundary volume. The bulk activation energies for BZY-Zn and pure BZY15 are similar, suggesting that incorporation of 1 wt% ZnO does not significantly affect the electrochemical properties of the sintered bulk material.

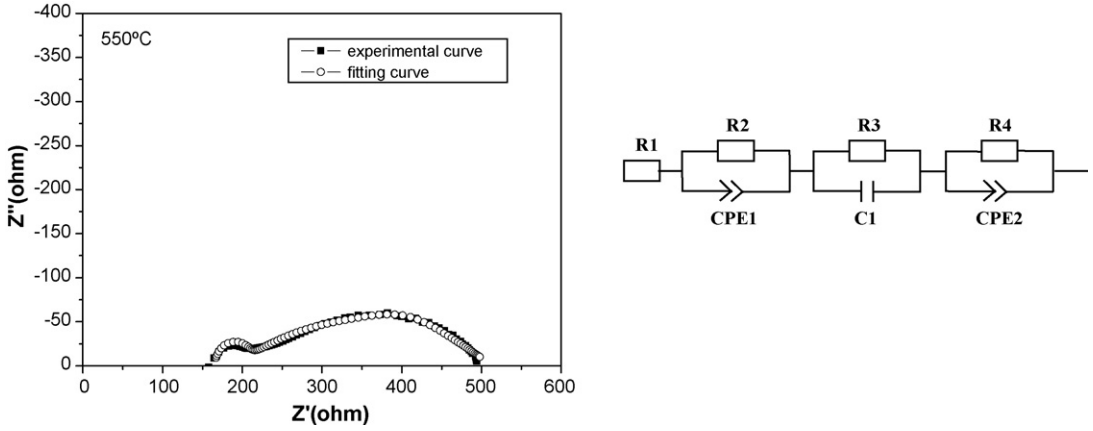

Fig. 3. Typical impedance spectrum at 550 °C and equivalent circuit for BZY-Zn.

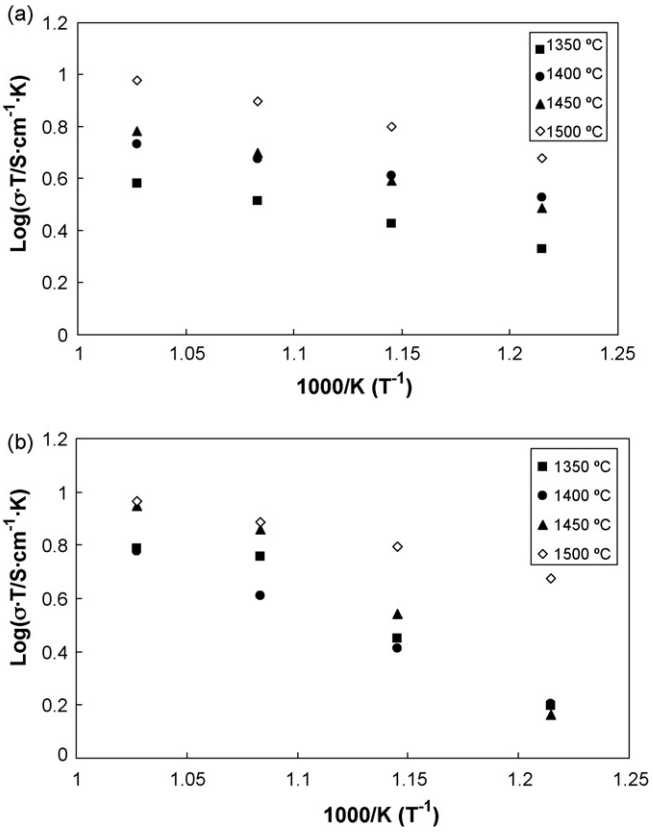

Fig. 4. Comparison of (a) bulk and (b) grain boundary conductivities in humidified (3% H_2O) 5% H_2 atmosphere for BZY-Zn electrolyte sintered at different temperatures (1350–1500 °C).

3.2. Performance of electrolyte-supported fuel cell

The open circuit potentials for the hydrogen concentration cells at the temperature range of 500–800 °C were used to evaluate proton transport through the BZY-Zn electrolyte membrane. The obtained results are shown in the Fig. 5. According to our measurements, BZY-Zn electrolyte has rather high proton transport numbers in the tested temperature range with the decreasing trend at high temperatures (about 0.85 at 800 °C).

Current–voltage (I–V) curves for the electrolyte-supported (1 mm thick) single fuel cell using hydrogen as fuel at different temperatures are shown in Fig. 6. The cell was stabilized at different temperatures to study the effect of temperature on the electro-

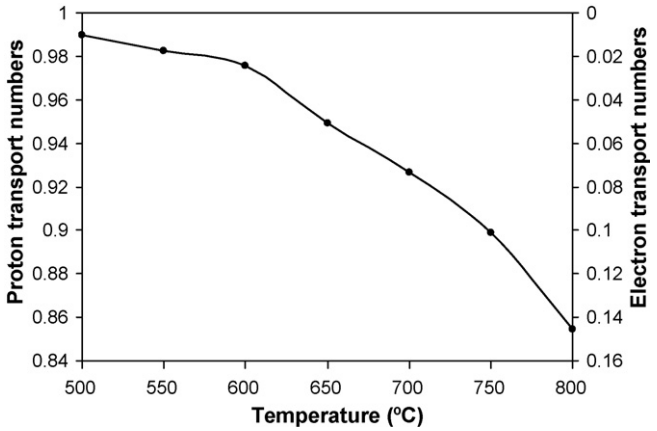

Fig. 5. Proton transport numbers of BZY-Zn electrolyte.

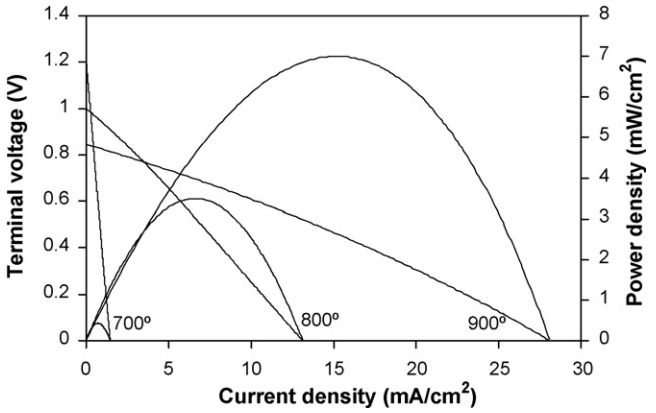

Fig. 6. Performances of H_2–O_2 fuel cell using thick (1 mm) BZY-Zn electrolyte at different operating temperatures.

chemical properties of BZY-Zn electrolyte material. The open circuit voltage was steady at ca. 1.2 V at 700 °C, indicating good sealing and no leakage into the sample cell. The decrease in the OCV with an increase in temperature was close to that predicted with Nerst equation. The slope of the I–V curves decreased with increasing temperature, which indicated an improvement in the overall performance of the cell. The slope in the I–V plot represented a combination of ohmic resistance present in the cell and electrode polarization resistance.

It is known that over-potential of Pt electrodes decreases sharply with temperature due to contributions to the complex electrochemical electrode reactions involving activation and diffusion of hydrogen and oxygen. Increasing the temperature is likely to accelerate the electrochemical reaction and thereby decrease the over-potential. However, it is obvious from the above data that the ohmic resistance of thick BZY-Zn electrolyte was too high to achieve good performance even at such high temperatures as 800 °C and 900 °C. Therefore development of thin films of electrolyte is essential for the application of IT-SOFCs based on BZY-Zn materials. Consequently, a systematic investigation was conducted to develop electrode-supported assemblies with thin films of BZY-Zn electrolyte, and thereby to enhance the performance of fuel cells.

3.3. Performance of cathode-supported fuel cell

During the firing process, substrates and coating thin films shrank by more than 10%. Differential shrinkage caused difficulties in obtaining flat integral membranes. Camber, delaminating, and cracks were caused by the mismatched sintering shrinkage of the different materials. The effect of sintering process conditions on the shrinkage values of porous substrates was investigated. The process variables investigated were thickness, diameter of the membrane and sintering temperature. The shrinkage of the samples in the lateral direction was always much higher than that in the thickness. As shown in Fig. 7, the linear shrinkage increased up to about 20% with sintering temperature to 1450 °C, and thereafter there was no further shrinkage. The linear shrinkage of dense BZY-Zn pellets prepared by dry pressing method was about 17% at 1500 °C. Therefore there were some differences between the above results based on the porous substrates and those for dense electrolyte film. Hence, as the shrinkage rate of the substrate was larger than that of the thin film during sintering, it was necessary to first partially pre-sinter the substrate.

The cross section morphology after co-sintering of BZY-Zn thin film deposited on porous [$(La_{0.8}Sr_{0.2})_{0.98}MnO_{3-\delta}$ + BZY-Zn] substrate (LSM20 from NexTech Materials) is shown in Fig. 8. The SEM and EDX analyses show that the dense surface layer of BZY-Zn elec-

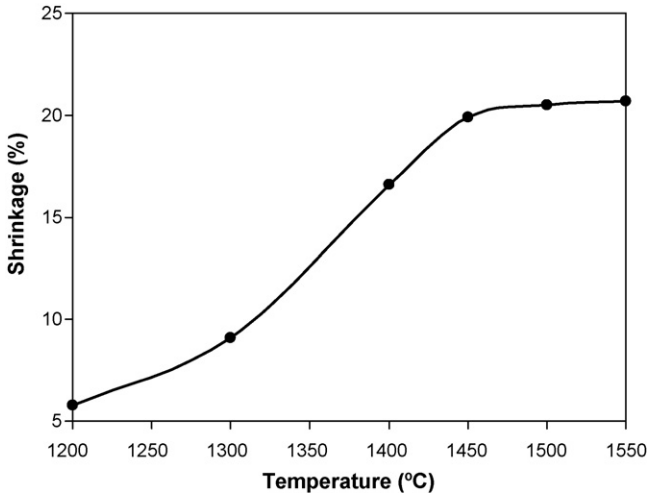

Fig. 7. Dependence of linear shrinkage of porous LSM + BZY-Zn substrate on sintering temperature.

trolyte tightly connected to the porous substrate. The distribution was confirmed by EDX spectra of two different zones denoted as Pt #1 and Pt #2 in Fig. 8. The point closest to the porous area (Pt #2) belongs to the substrate and consists of BZY-Zn and LSM20 particles (EDX). The point closest to the surface in the dense layer (Pt #1) is the desired BZY-Zn thin film. There were some signals arising from LSM20 in the spectrum from the dense layer (Pt #1), which were attributable to one or both of an uneven surface and electronic scattering from surrounding material since the thin film was less than 10 μm.

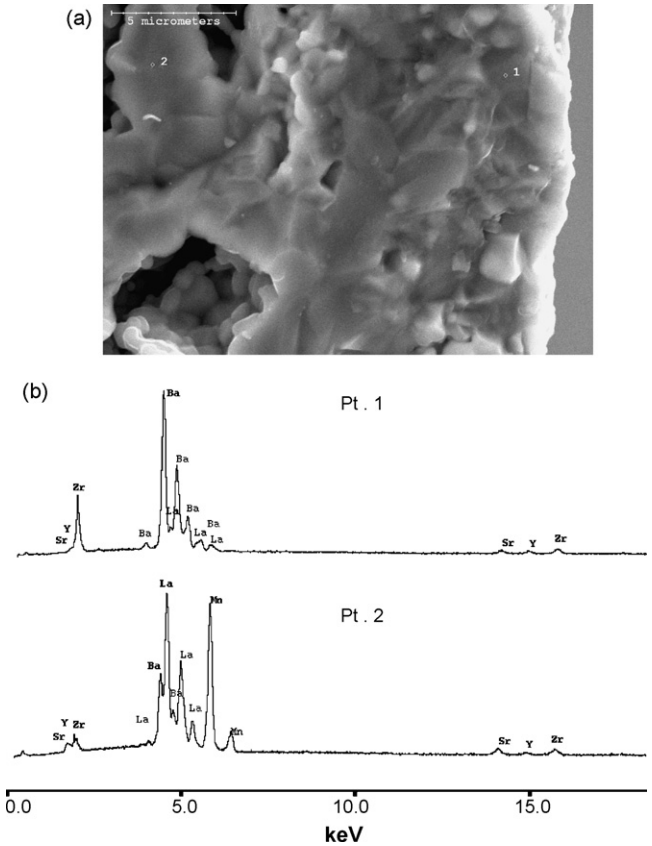

Fig. 8. Cross-sectional SEM image and EDX analyses of cathode-supported thin film electrolyte membrane after co-sintering.

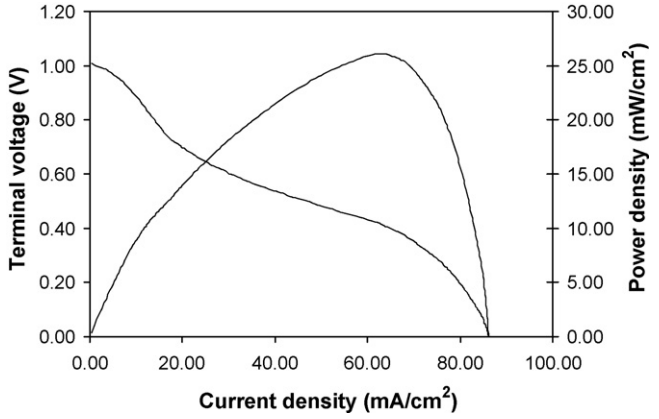

Fig. 9. Performance of H_2–O_2 fuel cell using cathode-supported BZY-Zn electrolyte at 800 °C.

Hydrogen fuel cell performance measurements were conducted using the cathode-supported BZY-Zn electrolyte at 800 °C. Contrary to our expectations, the maximum power density increased only about seven times comparing to that of the thick (1 mm) BZY-Zn electrolyte membrane. However, this result could be explained by high activation and mass transport losses in the cathode substrate as well as by relatively high total ohmic resistance, as shown by the shape of the current–voltage characteristic (Fig. 9). The total area specific ohmic resistance of the cathode-supported membrane was estimated to be ca. 4–5 ohm cm^2, resulting primarily from the substrate material's resistance (taking into account the relatively small resistance of thin electrolyte layer: ca. 0.1 ohm cm^2). Thus, in spite of the relatively low power density obtained, it is reasonable to conclude that there was a significant increase of operating efficiency of IT-SOFCs based on the BZY-Zn thin electrolyte provided with highly active and conductive supporting material. The data showed that, to improve efficiency of the cathode supporting material, we need to (i) increase its catalytic activity and ionic conductivity by doping and composition optimization and (ii) promote mass transport processes by optimization of pore size distribution. These issues are under investigation now in our research group.

4. Conclusions

The electrochemical properties of dense ZnO-doped BZY15 membranes depend on sintering temperature in the range 1350–1500 °C. Samples sintered at 1500 °C have similar bulk activation energy to BZY15 sintered at 1650 °C, while the grains boundary activation energy is considerably lower than that of BZY15. Electrochemical performance of thick electrolyte membranes was very low even at high temperatures. To improve performance, cathode-supported thin film electrolyte assemblies were prepared successfully by use of a spin coating technique. Fuel cell performance of the cathode-supported 10 μm thin electrolyte improved seven-fold when compared to thick electrolyte membrane, but the improvement was not linearly proportional to the electrolyte thickness.

Acknowledgment

This work was supported by Natural Sciences and Engineering Research Council of Canada (NSERC) Strategic Project Grant.

References

[1] H. Iwahara, T. Esaka, H. Uchida, N. Maeda, Solid State Ionics 3–4 (1981) 359–363.
[2] H. Iwahara, T. Yajima, T. Hibino, K. Ozaki, H. Suzuki, Solid State Ionics 61 (1993) 65–69.

[3] T. Hibino, K. Mizutani, T. Yajima, H. Iwahara, Solid State Ionics 58 (1992) 85–88.
[4] H. Iwahara, Solid State Ionics 86–88 (1996) 9–15.
[5] T. Norby, Solid State Ionics 125 (1999) 1–11.
[6] K.D. Kreuer, Annu. Rev. Mater. Res. 33 (2003) 333–359.
[7] H.G. Bohn, T. Schober, J. Am. Ceram. Soc. 83 (2000) 768–772.
[8] K.D. Kreuer, S. Adams, W. Munch, A. Fuchs, U. Klock, J. Maier, Solid State Ionics 145 (2001) 295–306.
[9] M. Laidoudi, I. Abu Talib, R. Omar, J. Phys. D: Appl. Phys. 35 (2002) 397–401.
[10] K.D. Kreuer, Solid State Ionics 125 (1999) 258–302.
[11] F.M.M. Snijkers, A. Buekenhoudt, J. Cooymans, J.J. Luyten, Scr. Mater. 50 (2004) 655–659.
[12] K.D. Kreuer, E. Schönherr, J. Maier, Proceedings of the 14th Risø International Symposium on Materials Science, Risø National Laboratory, Roskilde, Denmark, 1993.
[13] D. Shima, S.M. Haile, Solid State Ionics 97 (1997) 443–455.
[14] K. Yamashita, K.V. Ramanujachary, M. Greenblatt, Solid State Ionics 81 (1995) 53–60.
[15] Y. Zhou, M.N. Rahaman, Acta Mater. 45 (1997) 3635–3639.
[16] M.L. Li, H. Liang, M.X. Xu, Mater. Chem. Phys 112 (2008) 337–341.
[17] T.S. Zhang, J. Ma, Y.L.B. Kong, P. Hing, Y.J. Leng, S.H. Chan, J.A. Kilner, J. Power Sources 124 (2003) 26–33.
[18] J. Li, T. Ikegami, T. Mori, Acta Mater. 52 (2004) 2221–2228.
[19] C. Kleinlogel, L.J. Gauckler, Solid State Ionics 135 (2000) 567–573.
[20] T.S. Zhang, J. Ma, Y.J. Leng, S.H. Chan, P. Hing, J.A. Kilner, Solid State Ionics 168 (2004) 187–195.
[21] J.S. Lee, K.H. Choi, B.K. Ryu, B.C. Shin, I.S. Kim, Ceram. Int. 30 (2004) 807–812.
[22] M. Pollet, S. Marinel, F. Roulland, G. Allainmat, Materials Sci. Eng. B104 (2003) 58–62.
[23] Y.C. Lee, W.H. Lee, F.S. Shieu, Jpn. J. Appl. Phys., Part 1: Regul. Pap., Short Notes Rev. Pap. 42 (3) (2003) 1311–1314.
[24] P. Liu, H. Ogawa, E.S. Kim, A. Kan, J. Eur. Ceram. Soc. 23 (14) (2003) 2417–2421.
[25] A.A. Hassan, O. Abdelal, S.M. El-Hout, J. Mater. Sci. Technol. 23 (2007) 131–134.
[26] R. Jose, A.M. John, J. Koshy, J. Amer. Ceram. Soc. 85 (10) (2002) 2389–2394.
[27] A.V. Orlov, A.L. Vinokurov, O.A. Shlyakhtin, Y.D. Tretyakov, Mendeleev Commun. 4 (2004) 163–165.
[28] Y.C. Lee, W.H. Lee, F.S. Shieu, Jpn. J. Appl. Phys. Part 1: Regul. Pap., Short Notes Rev. Pap. 41 (10) (2002) 6049–6053.
[29] Y. Wang, L. Li, J. Qi, Z. Gui, Mater. Chem. Phys. 76 (2002) 250–254.
[30] S. Tao, J.T.S. Irvine, Adv. Mater. 18 (12) (2006) 1581–1584.
[31] M. Liu, P. He, J.L. Luo, A.R. Sanger, K.T. Chuang, J. Power Sources 94 (2001) 20–25.
[32] J.X. Li, J.L. Luo, K.T. Chuang, A.R. Sanger, Electrochim. Acta 53 (10) (2008) 3701–3707.